Characterization of a Pressurized Feeder for Biomass Injection into Gas-Solid Systems

Lucas Massaro Sousa[1], Benjamin Amblard[1], Florian Montjovet[1], Sina Tebianian[1*]

[1]Process Design and Modeling Division, IFP Energies Nouvelles,

Rond-Point Échangeur de Solaize, 69360 Solaize, France

---

* Corresponding author. E-mail adresses : sina.tebianian@ifpen.fr (S. Tebianian),
lucasmassaro@estudante.ufscar.br (L. Massaro Sousa)

ABSTRACT

Injection of biomass powders into multiphase reactors is a challenging task that may impact the process yield and limit the operation due to the feeder's blockage or unstable flow. A horizontal pressurized gas-solid feeder is characterized in this study to inject a batch of biomass powders of different diameters into cold-flow model operating under single phase, and multiphase fixed and fluidized regimes. The gas-solid hydrodynamics in the injection line is investigated for different operating conditions, using a fast camera with acquisition rate of 3000 images/s. Stable injections are performed in a wide range of solids fluxes, and under different solid concentration flow conditions. The operation map for the feeder is produced, and the phenomena that produce difficulty of stable injection are discussed. Ultimately, this type of solids injector is useful for feeding powders into lab-scale reactors for mixing and kinetic studies and might be also scaled-up for treating waste biomass powders into pilot-to-industrial scale reactors under batch or semi-continuous operations.

Keywords: waste biomass; solids handling; pneumatic powder injection; fluidized bed.

1   Introduction

There is growing interest in using waste biomass powders, originated from agricultural residues or industrial processing, to produce renewable energy and fuels. Particularly, sawdust stands out as an important residue of saw-milling, wood, and paper industries that is produced in large quantities worldwide. Due to its availability, low ash content, and attractive energy density, this powder can be used as a solid fuel in the industry itself, hence enhancing the overall energy balance with environmental awareness [1–9].

Current thermochemical processes, such as pyrolysis, gasification, combustion, and chemical looping rely on efficient feeding of solid fuel particles into entrained, fixed or fluidized bed reactors. Thus, the performance of the conversion processes is inevitably linked to the design of the solid injection system. This system should be simple, provide stable operation with low energy consumption, controlled solids flowrate as a function of the operating variables, and provide flexibility in case of variations in solid fuel physical properties. Efficient solid injectors should assure a proper dispersion of the solid fuel into the reactor medium with no accumulation of powders near the connection to the reactor and be resistant to wear and seizure.

Common characteristics of waste biomass powders, such as low particle density, irregular shape, variable particle size distribution, and moisture content make the feeding of these powders into reactors a recurring challenge [10–15]. In practice, inefficient or poorly designed feeders provide unstable or no flow of solids to the reactor, compromising the process yield, stability, automation, and safety.

Pneumatic injection of solids into multiphase reactors is of interest in continuous processes due to improved bed penetration. Some efforts concerning powders injection into fluidized beds are described in the literature. Guedon et al. [16] performed inclined injections of a Geldart B, prepolymer powder into a pressurized fluidized bed. After analyzing the effect

of several operating parameters on the jet penetration, the mentioned authors concluded that pressurized gas pulses could be used to disperse solids into the reactor. Later on, a solid slug feeder was developed at the Institute for Chemicals and Fuels from Alternative Resources (ICFAR), Canada, based on the same principle of a pressurized gas pulse for carrying solids [17,18]. Stable solids flowrates and reliable operation are reported for a wide range of materials, classified as Geldart A (meat and bone meal, FCC catalyst, and sawdust), Geldart B (dried distilled grains), and Geldart D (Tucumã seeds, and nylon ball) [19–21].

Batch pneumatic injection of a given amount of solid into a multiphase system is of particular interest for lab-scale batch unit reactors for kinetic studies and cold-flow models for characterization of mixing hydrodynamics between the injected solid tracer and the reactor medium. Controlled and stable powder batch injection into a multiphase system is far from trivial and results in difficulties in performing parametric studies to assess the effect of operating conditions on system performance. In light of the mentioned challenges and encouraging results, additional research for quantitative characterization of batch injection of powders by gas pulses is of great interest. There are gaps in knowledge in assessing:

(i) The effect of the operating variables (e.g. gas pressure, and solids inventory) on the solids flux and gas-solid hydrodynamics in the injector.

(ii) The influence of the reactor's fluidization regime on the injector performance.

(iii) The effect of the powders' particle size distribution and density on the feeder performance.

(iv) The feasibility of solid injection in dilute or dense regime with the same system.

In this paper, batch transport and injection of sawdust powders are analyzed in detail using pressurized gas pulses. First, the solids flux, mean voidage, and gas-solid qualitative hydrodynamics at the injection line are assessed for different operating conditions. Then, the feeder's performance is compared for the injection of sawdust with different particle size

distributions and by feeding powders into systems operating under different fluidization regimes.

2   Material and Methods

2.1   Materials

Three sawdust samples with different particle size distributions were used as injection powders (S_1, S_2, and S_3) and one FCC catalyst (C) used as filling material of the reactor. The powders' physical properties are depicted in Table 1.

Table 1. Physical and bulk properties of the employed solids.

Powder	MC (%)	d_{10} (µm)	d_{50} (µm)	d_{90} (µm)	ρ_p (kg/m^3)	ρ_{lb} (kg/m^3)	ρ_{tb} (kg/m^3)	ε_{lb} (-)	ε_{tb} (-)
S_1	5.1	200	447	833	970	204	270	0.79	0.72
S_2	8.8	370	647	1100	1030	197	240	0.81	0.77
S_3	8.3	552	1130	2220	900	222	290	0.75	0.68
C	3.1	40	82	136	1180	735	840	0.38	0.29

The particle size distribution was determined by laser diffraction under a dry atmosphere with Malvern Mastersizer 3000. The diameters that represents 10, 50, and 90% of the cumulative size distribution on volume basis are shown in Table 1. The initial moisture content of the samples (MC) was obtained by the gravimetric method at 105 °C for 24 h.

The loose (ρ_{lb}) and tapped bulk densities (ρ_{tb}) were measured with the Autotap AT-2 equipment (Quantachrome Instruments) under 0 and 2000 taps, respectively. The particle density (ρ_p) was determined with a mercury pycnometer under the pressure of 0.212 MPa, which means that pores with a diameter smaller than 7 µm are not filled with Hg. The loose (ε_{lb}) and tapped (ε_{tb}) porosities were calculated from the ratio of bulk to particle densities, and powder beds with void fractions from 68 to 81% were observed for the sawdust samples regardless of their size distribution. These high values are typical of residue-based biomass powders, with void fraction usually ranging from 60 to 93% [22–26].

2.2 Solids feeding system and cold-flow unit

The experiments were conducted in a cold-flow unit equipped with a solid feeding system, as shown in Fig. 1. The injector consists of a 0.02 m-internal diameter pipe made of acrylic that is sealed from the injection line with a ball valve. The mass of solids (M) is stored within the injector that can be pressurized with compressed air (P) provided that the ball valve is closed. The absolute gas pressure in the chamber can be adjusted from 180 to 500 kPa, which is the safety limit to prevent rupture of the acrylic pipe.
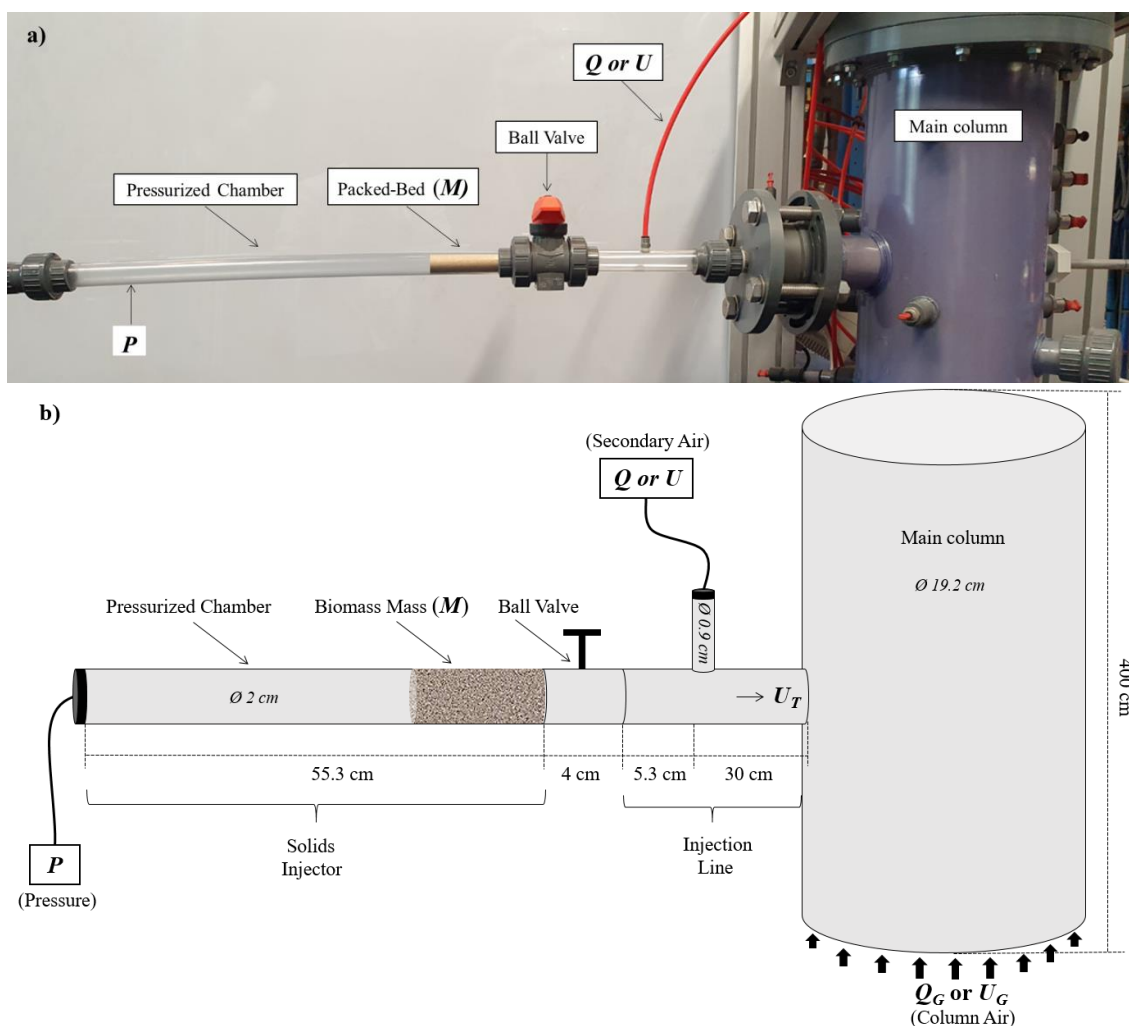
Fig. 1. Powders' injection system and principal variables investigated: P, M, Q or U, and Q_G or U_G. a) experimental unit and b) unit scheme with dimensions in cm as indicated.

By opening the ball valve, there is flow of solids to the main column as a gas-solid pulse, depending on the initial combination for pressure (P) and biomass mass (M). Both the qualitative behavior of the pulse, and the solids flux were assessed with a high-speed camera

(Fastcam APX RS) positioned at the injection line section (the marked region between the main column and the ball valve). The acquisition rate was set to 3000 images/s for all experimental conditions.

The solids mass flux (G_S) for each injection was calculated by:

$$G_S = \left(\frac{M - M_F}{A_1 . \Delta t}\right)$$

(1)

in which M is the mass of solids initially added to the feeder in kg, and M_F is the mass of remaining biomass in the injection line after the test; Δt is the flow time in seconds determined from the collected images (Section 3.1); and A_1 is the cross-sectional area of the injection line, equal to 3.14E-4 m^2.

The initial loading of the injector with air (V_A) and solids (V_S) with respect to non-pressurized conditions of the injector is given by:

$$V_A = \frac{\left(V - \frac{M}{\rho_p}\right) . \left(\frac{T_{ref}}{T}\right)\left(\frac{P}{P_{ref}}\right)}{V}$$

(2)

$$V_S = \frac{M}{V . \rho_p}$$

(3)

in which V is the volume of the pressurized chamber, equal to 1.73E-4 m^3, T and P are the gas temperature and gas pressure in K and kPa, respectively. The gas temperature was around 283.15 K in all experiments. T_{ref} is equal to 273.15 K and P_{ref} to 101.33 kPa. Note that the upper term in Eq. (2) converts the pressurized air to Nm^3, and the two injector operating variables are combined into one parameter (V_A). As shown in Eq. (2), V_A is higher by decreasing M or by increasing P.

Additionally, the initial loading of gas that occupies the region on the left side of the packed bed (V_A*) in the injector can be calculated by considering the mean bulk density between loose and tapped conditions (ρ_m) rather than ρ_p in Eq. (2):

$$V_A^* = \frac{\left(V - \frac{M}{\rho_m}\right) \cdot \left(\frac{T_{ref}}{T}\right)\left(\frac{P}{P_{ref}}\right)}{V} \tag{4}$$

A continuous secondary air flowrate (Q) from 0 to 6 Nm^3/h can be perpendicularly inserted after the injector during the experiments. The velocity at the secondary injection (U) ranged from 0 to 26.2 m/s considering the cross-sectional area (A_2) of 6.36E-5 m^2. The total air velocity (U_T) to the main column, as marked in Fig. 1, is calculated by:

$$U_T = \frac{\left(V - \frac{M}{\rho_p}\right) \cdot \left(\frac{T_{ref}}{T}\right)\left(\frac{P}{P_{ref}}\right) + U.A_2.\Delta t}{A_1.\Delta t} \tag{5}$$

The secondary air contribution on U_T compared to the pressurized air is given by:

$$X = \frac{U.A_2}{U_T.A_1} \tag{6}$$

The mean void fraction to the main column (ε) can be iteratively estimated by:

$$\varepsilon = \frac{U_T}{U_T + U_S} = \frac{U_T}{U_T + \frac{G_S}{\rho_p(1-\varepsilon)}} \tag{7}$$

in which U_S is the calculated solids velocity. The mean solids fraction (ε_s) is calculated by:

$$\varepsilon_s = 1 - \varepsilon \tag{8}$$

Finally, air flowrate can be homogeneously added to the bottom section of the main column through a perforated distributor plate (Q_G), from 0 to 80 Nm^3/h. The air velocity (U_G) ranges from 0 to 0.77 m/s, considering the column cross-sectional area is 0.0290 m^2.

2.3 Experiments planning

The summary of the experimental runs is shown in Table 2, with each test performed in triplicate. More specifically, experiments 1 to 8 were designed to understand the effect of M, P, and U on G_S and ε_s. Additional experiments were performed with sample S_2, in the range of $180 \leq P \leq 500$ kPa, and $0.003 \leq M \leq 0.026$ kg to build up an operation map of the viable injections with this feeding system (tests 20 to 29).

The performance of the injection system was also evaluated by changing powders' mean diameter (tests 9 to 12); by feeding of powders into a single-phase gas unit under different U_G's (tests 13 to 15) and for injection of powders into the unit operating under fixed and fluidized bed regime (tests 16 to 19). The static bed height of catalyst (C) in the unit was set to 1.05 m above the perforated plate (0.33 m above the injection line). The detailed experimental data (Δt, V_A, R, X, U_T, G_S, and ε_s) for each experimental condition is presented in Table A1 in Appendix A.

Table 2. Summary of the injection experiments.

Tests	Powder	P (kPa)	M (kg)	U (m/s)	U_G (m/s)	Catalyst presence in main column
1	S_2	300	0.003	0	0	-
2	S_2	300	0.006	0	0	-
3	S_2	300	0.012	0	0	-
4	S_2	300	0.012	4.4	0	-
5	S_2	400	0.012	4.4	0	-
6	S_2	500	0.012	4.4	0	-
7	S_2	300	0.012	17.5	0	-
8	S_2	300	0.012	26.2	0	-
9	S_1, S_3	300	0.003	0	0	-
10	S_1, S_3	300	0.012	4.4	0	-
11	S_1, S_3	300	0.012	17.5	0	-
12	S_1, S_3	400	0.012	4.4	0	-
13	S_2	300	0.012	17.5	0.29	-
14	S_2	300	0.012	17.5	0.48	-
15	S_2	300	0.012	17.5	0.77	-
16	S_2	300	0.012	17.5	0	Yes
17	S_2	300	0.012	17.5	0.14	Yes
18	S_2	300	0.012	17.5	0.29	Yes
19	S_2	300	0.012	17.5	0.48	Yes
20	S_2	180	0.003	0	0	-
21	S_2	200	0.003	0	0	-
22	S_2	250	0.003	0	0	-
23	S_2	400	0.003	0	0	-
24	S_2	500	0.003	0	0	-
25	S_2	300	0.018	0	0	-
26	S_2	500	0.018	4.4	0	-
27	S_2	500	0.024	4.4	0	-
28	S_2	500	0.026	4.4	0	-
29	S_2	200	0.006	0	0	-

3   Results and Discussion

3.1   Qualitative flow behavior

The hydrodynamics of the gas-solid injections are presented in Fig. 2, in which seven sequential flow behaviors were classified and explained in topics (a) to (g) as shown below. Note that the main parameter that enhances the movement of powder is the pressurized gas while the secondary aeration (U) contributes to different gas-solid hydrodynamics patterns in the injection line. Qualitatively, Fig. 2a to 2g-I represent the hydrodynamics of powder injections with $U{\neq}0$ m/s, whereas Fig. 2a to 2g-II for $U{=}0$ m/s:

 (a) Right after opening the ball valve, there is a dilute transport of solids at high speed from the pressurized chamber (left) to the unit (right).

(b) A slight increase in the solids concentration is visible; however, the transport remains qualitatively in a high-speed, dilute mode.

(c) A transition between dilute-to-dense flow is observed in the form of recurrent vertical layers with a low and high concentration of solids.

(d) A dense transport of solids takes place with no visible gas voids.

(e) A decelerating flow of solids is verified because of the decreasing drag force with the decrease of the pressurized chamber gas. Overall, the flow is in dilute mode with solids concentrated in the form of a tail, when $U{\neq}0$ m/s (Fig. 2e-I); or with solids homogeneously distributed along the tube, when $U{=}0$ m/s (Fig. 2e-II).

(f) For the conditions that $U{\neq}0$ m/s, the gas coming from the vertical inlet becomes predominant, with the formation of gas vortices and local turbulence at the injection line, hence the flow of solids exhibits two patterns: diluted flow to the unit and return of residual solids upstream the secondary air (Fig. 2f-I). For the conditions that $U{=}0$ m/s, the solids settle at the lower section of the tube, and their residual movement towards the unit is due to the powder's inertia (Fig. 2f-II).

(g) There is virtually no transport of powders to the unit, and the residual solids accumulate near the ball valve and on the pressurized chamber for $U \neq 0$ m/s due to the secondary air local turbulence (Fig. 2g-I), and throughout the base of the injection line for $U=0$ m/s (Fig. 2g-II).
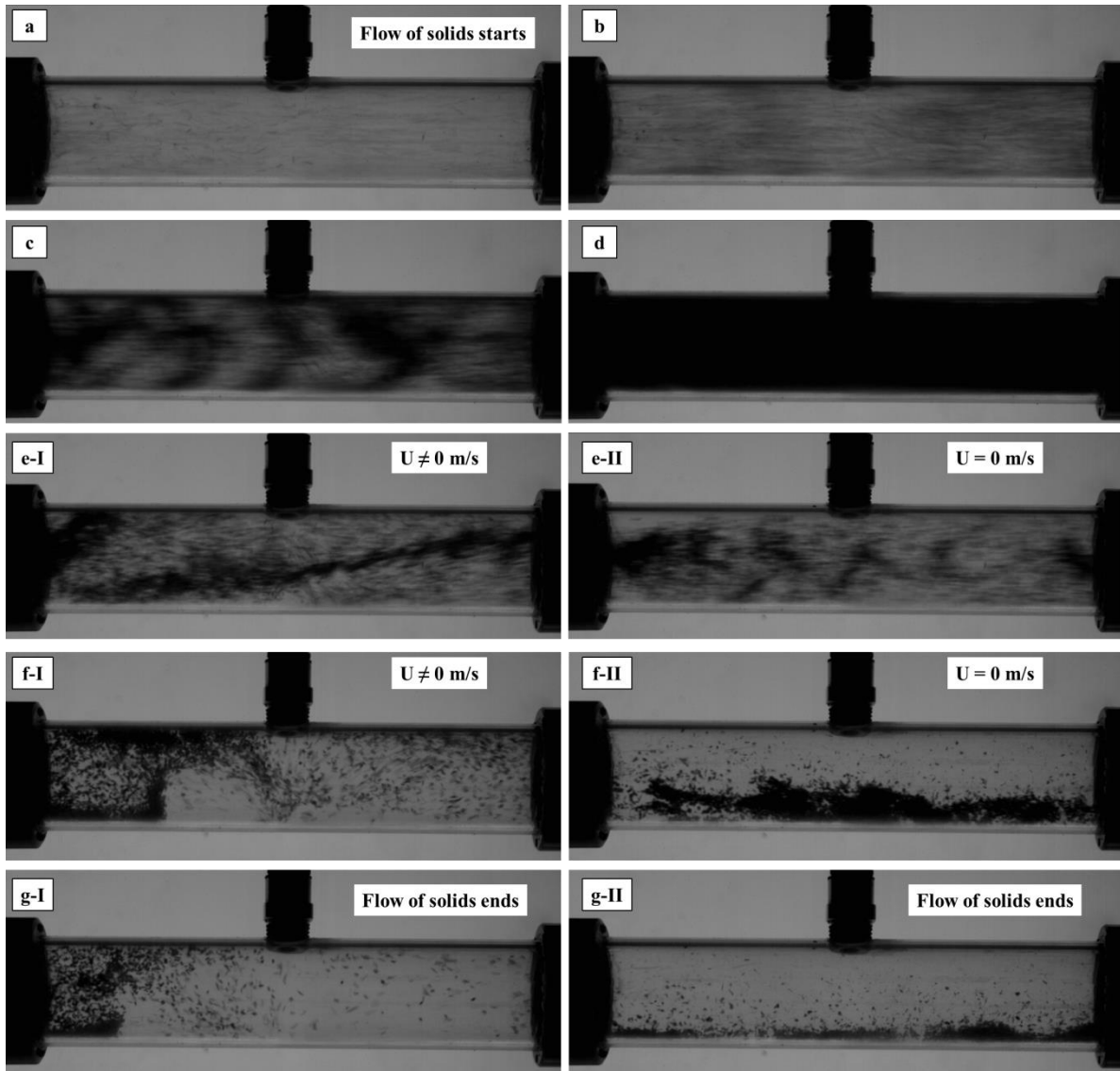
Fig. 2. Sequences of gas-solid hydrodynamics at the injection line for $U \neq 0$ m/s (Fig. 2a to 2g-I) and $U=0$ m/s (Fig. 2a to 2g-II).

The duration of each flow behavior and the total flow time depend on the initial injection condition. Thus, to prevent data bias and standardize the measurements, the flow time was averaged from condition (b) to the end of (e) for all assays. The mentioned conditions represent the time interval during which most of the solid is transported i.e. conditions in which qualitatively the solids mass flux to the unit in the injection line is not

negligible. In this way, the particularities of the injections are quantitatively encompassed in the solids mass flux (G_s), calculated from Eq. (1). The residual amount of powder in the tube (R) after the test is considered for the solid mass flux calculation. The solids injections are addressed quantitatively in the next sections, as a function of G_S and ε_s.

3.2 Effect of M, and P on G_S, and ε_s

The influence of the operating variables on G_S and ε_s is shown in Fig. 3, which corresponds to the results of tests 1 to 6 (Table 2). The accumulation of powders at the injection line was lower than 6% of M for all injections. Detailed data for each experimental condition can be found in Table A1 (Appendix A).
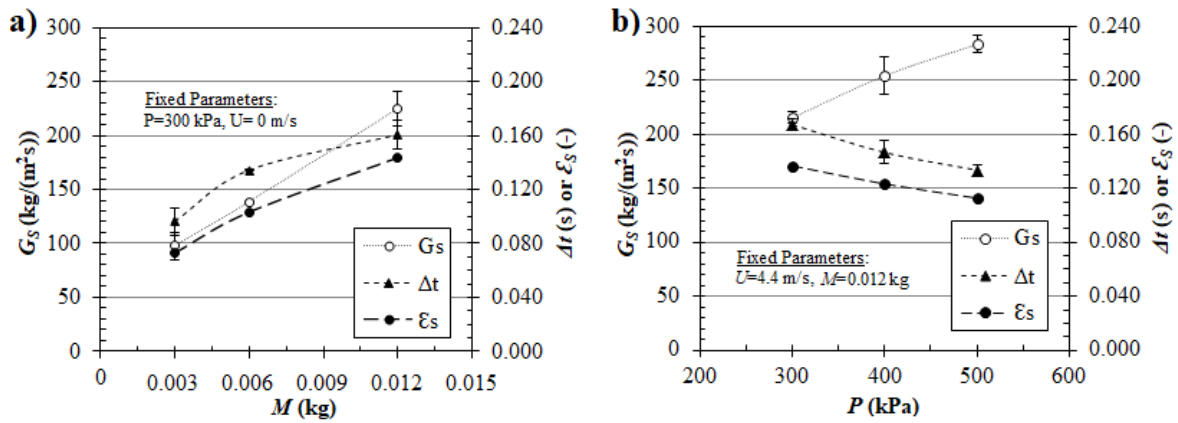
Fig. 3. Experimental solids flux (G_S), mean solids fraction (ε_s), and injection time (Δt) for sawdust S_2 as a function of operation parameters a) M, and b) P.

As shown in Fig. 3a, with this batch solid feeder, G_S is higher by increasing the initial mass of powders because the injections occur in a denser regime (higher ε_s) consequently with better usage of the gas momentum. In other words, the gas drag force is sufficient to push 3, 6, or even 12g of sawdust with a similar velocity but the flow is more concentrated for the latter. Note that flow condition (d) (Fig. 2), which relates to denser region of solids transport, becomes predominant as M increases. In Fig. 3b, the higher the pressure in the injector, the greater the quantity of gas for dragging solids to the unit, hence there is a decrease of the flow time with a consequent increase of solids mass flux.

By definition, the solids mass flux in a multiphase flow can be enhanced by increasing the solids concentration (ε_s) and/or the solids velocity (U_S) (Eq. 9). In summary, manipulating the operating variables M or P are straightforward ways to majorly act on ε_s or U_S, respectively.

$$G_S = \rho_p \varepsilon_S U_S \tag{9}$$

The solids flux is plotted as a function of the total air volume and air velocity in Fig. 4, which corresponds to the same data previously shown in Fig. 3 (tests 1 to 6). The pressurized gas volume in the injector decreases as M increases (from 0.003 to 0.012 kg), hence V_A and U_T also decrease as shown by the filled square data in Figs. 4a and 4b, respectively. The data suggest that there is a limiting condition in which powders are not dragged out of the pressurized chamber, which will be further discussed in the next section.

The increase of V_A and U_T with increasing P (from 300 to 500 kPa) is presented by empty triangle symbols in Figs. 4a and 4b, respectively. Although a slight flow dilution flow (ε_s) occurs under enhanced P (Fig. 3b), the flow concentration is more drastically affected by changing M (Fig. 3a).
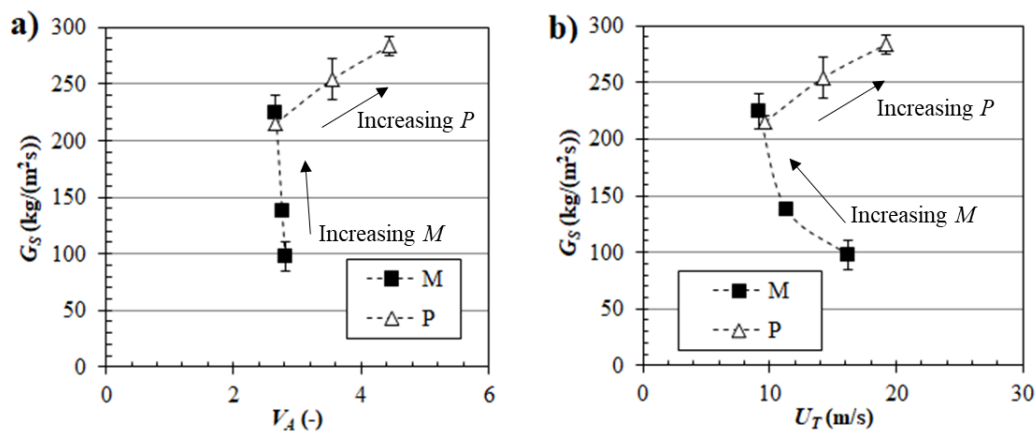
Fig. 4. Experimental solids flux (G_S) as a function of a) V_A, and b) U_T.

In the next section, the results of additional injections with sample S_2 are shown under $180 \leq P \leq 500$ kPa, and $0.003 \leq M \leq 0.026$ kg (tests 1 to 6, and 20 to 29). The aim is to produce an operating map of viable injections with the actual feeder and understand the phenomena that prevent a wider operation range.

3.3   Feeder operation region

The solids mass flux is plotted as a function of the total air volume in Fig. 5a. The trends of the curves are similar to those previously shown in Fig. 4a, for tests performed with different M (filled square symbols), and different P (empty triangles). Since the effect of the operating variables on G_S is already described in Section 3.2, the experimental data are hidden in Fig. 5c, and different regions were delimited.
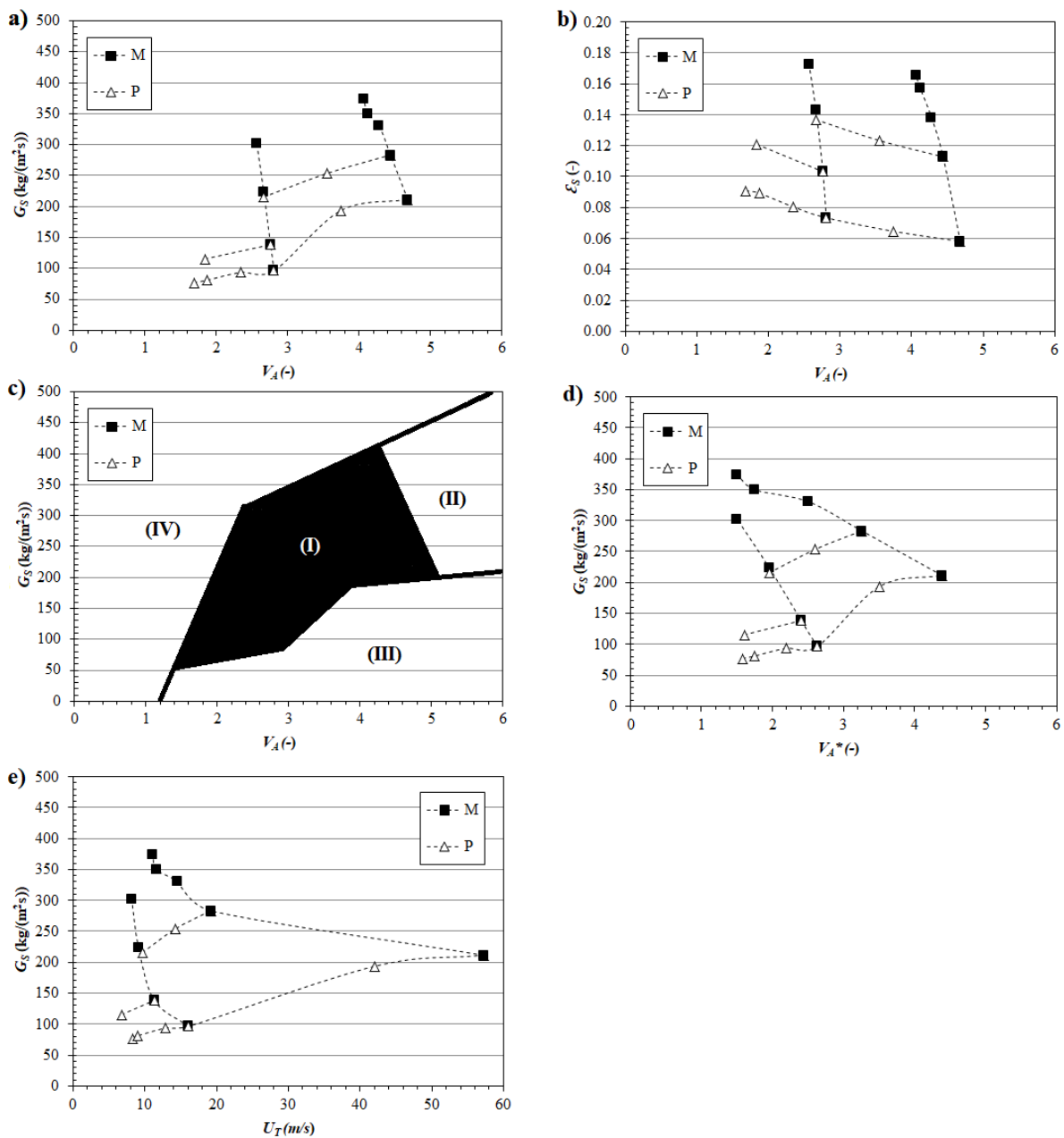
Fig. 5. Experimental data for injection of sawdust S_2: a) G_S versus V_A, b) ε_s versus V_A, c) operation map, d) G_S versus $V_A{}^*$, and e) G_S versus U_T.

The operation region of the actual solids feeder is shown in Region (I), in which injections with G_S from 60 to 400 kg/(m^{2}s) can be stably performed. The mentioned region of stable injection may be enlarged towards Region (II), by increasing P which was limited to 500 kPa in this study. Another alternative is extending the length of the pressurized chamber as more gas would be available to push the solids out of the pressurized chamber. Qualitatively, the gas-solid flow behavior at the injection line agrees with the proposed classification and sequence of images shown in Fig. 2, throughout Region (I).

Powder injection is not possible in Regions (III) and (IV) as explained below.

At the boundary between Regions (I) and (III), the solids to air ratio is lower and the injections occur in a more dilute condition, with $\varepsilon_s \leq 0.08$ as shown in the lower curve of Fig. 5b. The injection of powders with the combination of G_S and V_A shown in Region (III) is not viable for two reasons: i) reducing ε_s or G_S by further decreasing M is not reasonable because the initial mass of solids is already critically low (M=0.003 kg). In this condition, the volume occupied by solids in the pressurized chamber is of only 8% of the total chamber volume (calculated by Eq. (3) with ρ_m). Moreover, a significantly small amount will not be representative for hydrodynamic study of injection into fluidized beds; ii) increasing P over 500 kPa increases V_A, hence the boundary curve is prolonged towards Region (II) as marked in Fig. 5c. Qualitatively, the gas-solid flow behavior agrees with that shown in Fig. 2, however flow condition (d) (Fig. 2d) that represents the denser transport of solids is not verified. Consequently, flow behavior migrates from (c) (Fig. 2c) directly to (e) (Fig. 2e-I or 2e-II). This is quantitatively evidenced by the lowest values for ε_s.

At the boundary between Regions (I) and (IV), the solids to air ratio is greater and the injections occur in a denser mode with ε_s over 0.15, as presented in Fig. 5b. Qualitatively, the gas-solid flow behavior agrees with that shown in Fig. 2 and flow condition (d) (Fig. 2d) becomes more pronounced as the boundary between Regions (I) and (IV) is approached. This

is quantitatively evidenced by the highest values for ε_s. In Region (IV), the transport of sawdust is not viable because the pressurized gas is not sufficient to overcome the packed bed inertia in the injector and most of the solids remain in the injection line.

Following consideration may, at least in part, explain this limit of operation: As shown in Table 1, sawdust has high porosity beds and the limitation of its transport as M increases might be related to the distribution of air in the pressurized chamber (Fig. 1b). The hypothesis is that, in the pressurized chamber, the portion of air located on the left side of the packed bed is more important to push the powders to the unit than the gas that is pressurized within the bed of particles. Therefore, the operation map plotted as a function of V_A^* (Eq. 4) in Fig. 5d suggests that the transport of sawdust is not viable for V_A^* lower than 1.4 with the actual feeder. Future studies should investigate the effect of powder properties and injector dimensions on threshold values for V_A^* to avoid feeder malfunction.

Finally, in Fig. 5e, the solids flux data is presented as a function of the total velocity at the injection line, since U_T might be a limiting factor for certain processes. Stable feeding of sawdust is possible within $6.5 \leq U_T \leq 58.0$ m/s using the actual feeder and operating conditions.

3.4   Effect of U on G_S and ε_s

The secondary aeration is located after the injector, and it affects the qualitative gas-solid flow behavior in the injection line, as shown in Section 3.1. Quantitatively, G_S increases with increasing gas velocity U due to the decrease of the flow time (Fig. 6a).
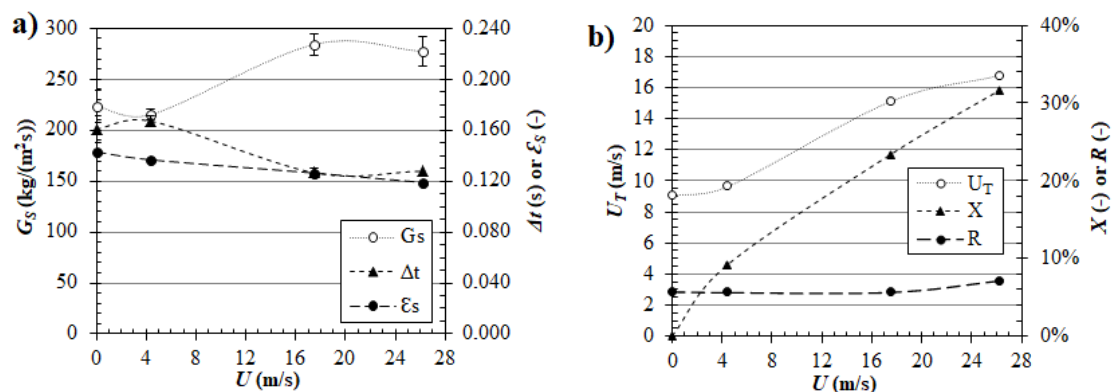
Fig. 6. Effect of U on a) G_S, ε_s, and Δt, and on b) U_T, R and X.

The reduction of the flow time is a consequence of the enhanced perpendicular drag force, observed under high aerations ($U>17.5$ m/s), that both accelerates the powders at the injection line to the main column, and also accelerates the establishment of flow condition (f) (Section 3.1). Under these conditions, the contribution of the secondary air to the total velocity (X) is higher than 20% (Fig. 6b) which justifies the enhanced turbulence in the injection line, and consequently the earlier interruption of the tail of flowing solids (Fig. 2f-I). In Fig. 6b, note that U_T increases with U as per Eq. (5) and that solids accumulation is not greatly influenced by increasing U (R increases from 5.7 to 7%). The amount of residual powders in the line can be reduced by using higher gas pressure (P), for example, as per tests 4-6 (Table A1).

For low secondary gas velocities ($U=4.4$ m/s), G_S is similar to that of conditions without secondary gas but without accumulation of powders on the injection line. Thus, the values of G_S in the operation map (Fig. 5c) are directly valid for $0 \leq U \leq 4.4$ m/s.

3.5   General recommendations for feeder operation

In the previous sections, it was shown that batch injection of powders is possible in a wide range of solids mass fluxes and under different gas-solid concentrations with this solid's feeder. From a practical perspective, the best strategy to set ε_s to desired targets (i.e., achieve more dilute or dense flow conditions) is by manipulating M with this injector. On the other hand, if greater amounts of solids must be injected in one batch, P should be manipulated to widen the operation. It is also recommended to maintain a continuous secondary gas velocity at the injection line to prevent backflow of solids from the unit to the injection line, and to minimize risks of spontaneous combustion in the injection line, for high-temperature processes. Although U might be used for fine-tuning of G_S, as shown in Fig. 6a, it is most important to prevent the accumulation of powders in the injection line.

Some analogies between mechanical and non-mechanical solids feeders are found in the literature, for example, those relating the operation of L-valves with slide and butterfly valves [27,28]. The working principle of the solid's injector addressed here can be related to the expansion of a gas pushing a piston, which is a typical thermodynamics exercise. In this case, the piston is the packed bed that is pushed by the gas due to the pressure difference between the injector and injection line, which is observed when the ball valve is opened. Note that the pressure-volume work on the piston in thermodynamics is encompassed in Eqs. (2) and (4) by considering the quantity of gas in Nm^3 (i.e., gas pressure multiplied by gas volume). This is the reason that the operation map in Fig. 5 is plotted as a function of V_A or V_A^*, which are the driven forces for the solids transport with this equipment.

Future studies should focus on some geometrical parameters to widen the feeder operating region, such as pressurized chamber diameter, length and angle, and on developing scale-up rules for the injector in continuous operation.

3.6   Estimating G_S for different operating conditions

The solids flux under different P and M can be estimated by interpolating the curves of known conditions in Fig. 5a, however, some correlations are proposed here to speed up the process and calibrate future experiments.

The procedure consists of calculating V_S/V_A with Eqs. (2) and (3) for a given P and M. Note that V_S/V_A represents the initial loading of solids compared to the volume of air. Then, ε and Δt can be estimated with the correlations shown below, which were fitted to experimental data under 16 different conditions (tests 1-6 and 20-29 in Fig. 7a):
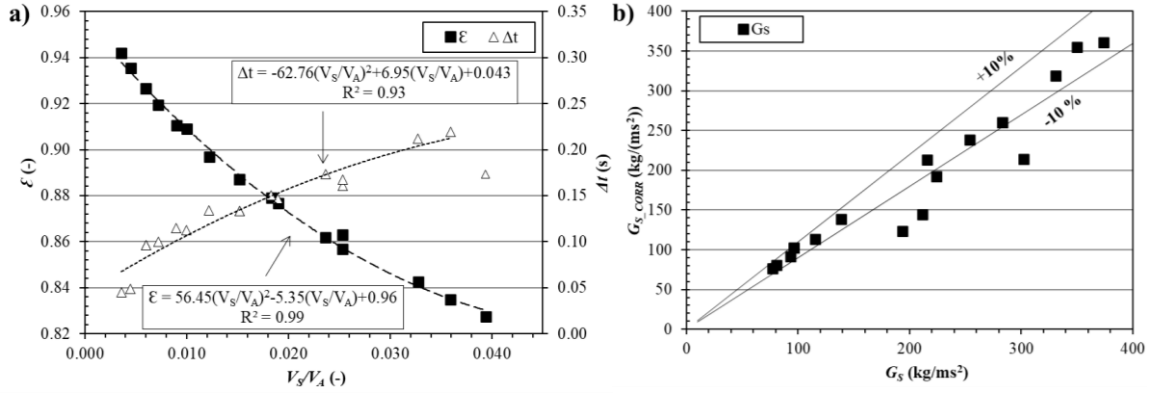
Fig. 7. Results for a) ε versus V_S/V_A, and b) fitting response for G_S.

$$\varepsilon = 56.45(\frac{V_S}{V_A})^2 - 5.35\frac{V_S}{V_A} + 0.96 \tag{10}$$

$$\varDelta t = -62.76(\frac{V_S}{V_A})^2 + 6.95\frac{V_S}{V_A} + 0.043 \tag{11}$$

Eqs. (10) and (11) are valid for the actual feeder within the limits $180 \leq P \leq 500$ kPa, $0.003 \leq M \leq 0.026$ kg, and $0 \leq U \leq 4.4$ m/s. Finally, with U_T calculated from Eq. (5), G_S can be estimated from the rearrangement of Eq. (7), as shown below:

$$G_S = \frac{\rho_p(1 - \varepsilon)^2 U_T}{\varepsilon} \tag{12}$$

The deviations between estimated and experimental G_S are generally smaller than 10% with this procedure, as shown in Fig. 7b. Only three points exhibit deviations in G_S of 30%, which corresponds to the operating boundaries of the injector ($\varepsilon \geq 0.93$, and $\varepsilon \leq 0.83$, tests 23 to 25) whose fitting of Eq. (11) is not so accurate. The correlation represents a calibration curve for predicting the behavior of the injector. Future studies could focus on developing more generalized mechanistic correlations valid for different injector diameters and operating conditions.

3.7   Injection of sawdust with different mean particle sizes

In this section, the performance of the injection system is evaluated in feeding sawdust samples with different particle-size distributions. The solids mass flux and residual mass of solids at the injection line ($R=M-M_F$) are shown in Fig. 8a and 8b, respectively, under various

operating conditions (tests 9 to 12). The solids mass flux and R for the finer sample (S_1) are similar to that of sample S_2 in all conditions; hence the operation map shown in Fig. 5 is also valid for $447 \leq d_{50} \leq 647$ μm.

The feeder's performance is reduced when injecting the coarser sample (S_3), due to enhanced powder interlocking effect and higher d_{50}/D, which results in partial clogging of the ball valve orifice under some experimental conditions. For example, for test 10 and 11, it is observed a decrease in G_S and an increase in R due to this clogging phenomenon. Visually, the restrictive Region (IV) in Fig. 5c would be larger with S_3, hence narrowing Region (I).
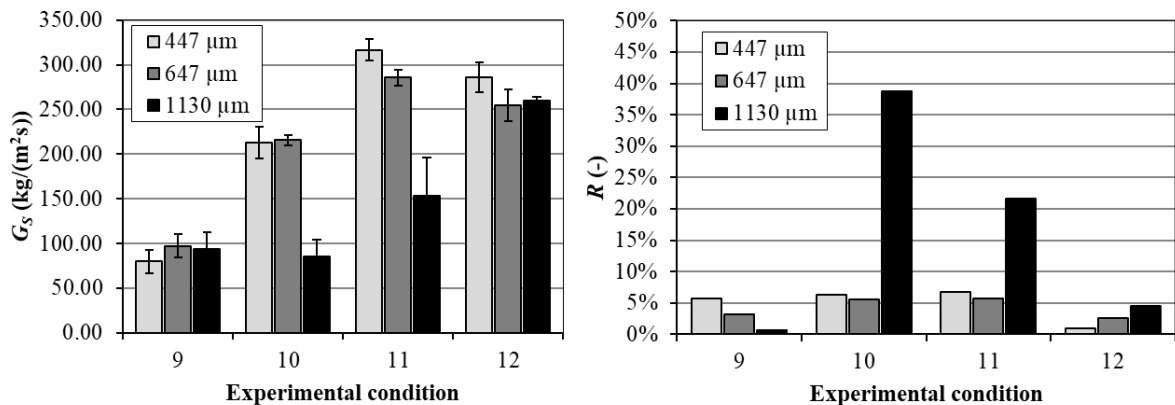
Fig. 8. Results of a) solids flux (G_S) and b) residual mass of solids (R) for the injection of three sawdust samples under different experimental conditions.

Nevertheless, the clogging issue can be solved by performing injections with a lower mass of solids (test 9) or by using higher gas pressures (test 12) to break up interlocking arches. As shown in Fig. 8, the solids mass flux and R with sample S_3 matches that of sample S_2 in test 9 and 12. Thus, the injector is suitable for handling sawdust powders of $447 \leq d_{50} \leq 1130$ μm, which is a common size range for this residue in industrial practice.

3.8   Injection of sawdust to single-phase gas unit

The effect of U_G on G_S was assessed with tests 7, and 13 to 15. Considering the standard deviations of the solids mass flux measurements, as given in Fig. 9 there is no significant difference for G_S as a function of U_G. This is an important result concerning the injector's robustness, as powders can be introduced into pneumatic transport lines consisting of carrier

gas or very dilutes regions of reactors without disturbance of the feeders' performance, even at high gas flowrates in the unit. Therefore, the operation map shown in Fig. 5 is also valid for the feeding of sawdust powders to units operating under extremely dilute pneumatic regime.
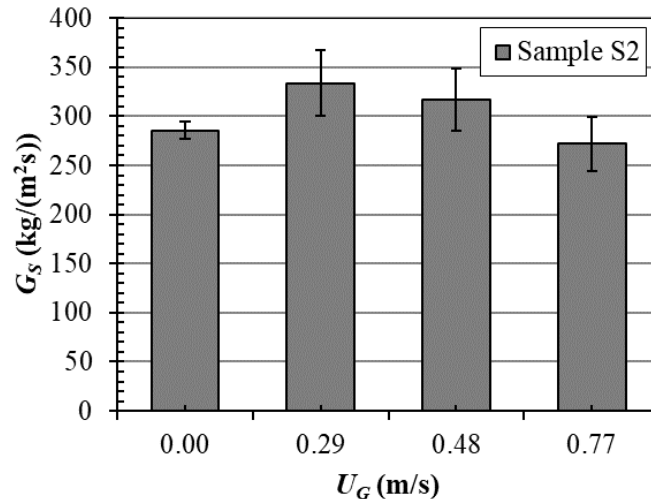
Fig. 9. Solids flux (G_S) for the injection of S_2 under different gas velocities in the unit (U_G).

3.9   Injection of sawdust into fixed and fluidized beds

In Fig. 10, solids fluxes are presented for injections of sample S_2 into fixed beds (U_G=0 m/s) and fluidized beds under different U_G (tests 16 to 19). The main column was filled with catalyst and operated under bubbling to slugging fluidization regimes according to Bi and Grace's diagram [29]. Considering the standard deviations, the solids mass fluxes are similar among the experiments with this injection system. Moreover, the G_S shown in Fig. 10 is similar to that of the injection of sawdust into a single-phase unit without catalysts (G_S=285±9 kg/(m²s), test 7). In conclusion, the operation of the solid's injector is not influenced by fixed or fluidized bed resistances. Therefore, although a slight increase of the restrictive Region (IV) is likely, the operation map (Fig. 5) remains valid for the feeding of sawdust powders to fixed and fluidized beds.
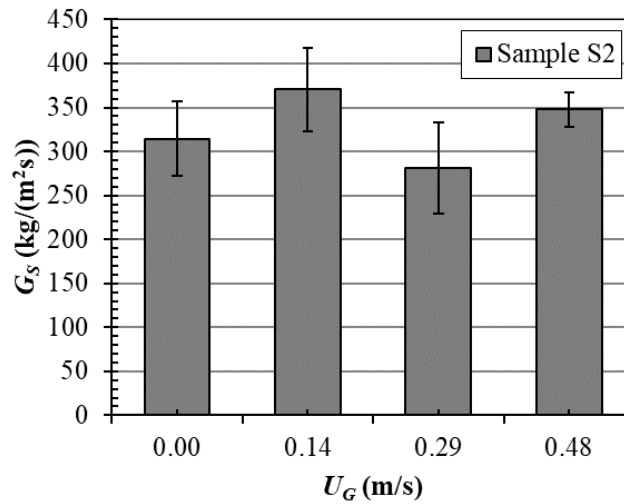
Fig. 10. Solids flux (G_S) for the injection of S_2 to fixed and fluidized beds under different unit gas velocities (U_G).

4   Conclusions

This paper reports successful application of a pressurized pneumatic solids feeder to inject a batch of waste biomass powders into fixed and fluidized bed reactors, as well as pneumatic transport lines. With this feeding system, sawdust powders could be stably injected in a wide range of solids mass fluxes, $60 \leq G_S \leq 450$ kg/(m^{2}s), and under more dilute or dense flow conditions, $0.83 \leq \varepsilon \leq 0.94$. The feeder is of easy operation, has low construction costs, and can quickly adapt to the process needs since injections with different G_S might be performed sequentially. Reported information is of particular interest for promoting reproducible batch injection of powders into lab-scale reactors focused on kinetic studies or for understanding gas-solid mixing and jet penetration in fluidized beds. It is also useful for researchers and engineers that handle solid waste biomass, for example, for renewable energy and fuel generation. Future studies will address the validation of numerical models for pressurized gas-solid injection, scale-up rules for the injector for continuous injection, and feeding of powders with different properties, such as moisture content and particle density.

Nomenclature

A_1	Cross-sectional area of the injection line (m^2)
A_2	Cross-sectional area of the secondary air inlet (m^2)
d_{10}	Volumetric diameter for 10% of samples' particle-size (µm)
d_{50}	Volumetric diameter for 50% of samples' particle-size (µm)

d_{90}	Volumetric diameter for 90% of samples' particle-size (µm)
G_S	Solids flux (kg/(m²s))
G_{S_CORR}	Solids flux predicted by Eqs. (10) to (12) (kg/m²s)
M	Initial mass of solids (kg)
M_F	Accumulated mass of solids (kg)
MC	Moisture content on a wet basis (%)
P	Air pressure at the injector (kPa)
P_{ref}	Reference air pressure (kPa)
R	Residual mass of solids (%)
T	Air temperature at the injector (K)
T_{ref}	Reference air temperature (K)
Q	Air flowrate in the injector (Nm³/h)
Q_G	Air flowrate in the unit (Nm³/h)
U	Secondary air velocity (m/s)
U_G	Air velocity in the unit (m/s)
U_T	Total air velocity (m/s)
V	Volume of the pressurized chamber (m³)
V_A	Initial volume of air defined in Eq. (2) (-)
V_S	Initial volume of solids defined in Eq. (3) (-)
$V_A{}^*$	Initial volume of air defined in Eq. (4) (-)
X	Variable defined by Eq. (6) (%)

Greek letter

Δt	Flow time (s)
ε	Mean flow void fraction (-)
ε_s	Mean flow solid fraction (-)
ε_{lb}	Loose void fraction (%)
ε_{tb}	Tapped void fraction (%)
ρ_{lb}	Loose bulk density (kg/m³)
ρ_m	Mean density between loose and taped conditions (kg/m³)
ρ_p	Particle density (kg/m³)
ρ_{tb}	Tapped bulk density (kg/m³)

References

[1]   C. Moliner, F. Marchelli, E. Arato, Current Status of Energy Production from Solid

Biomass in North-West Italy, Energies. 17 (2020) 4390.

[2]   P. McKendry, Energy production from biomass (part 1): overview of biomass,

Bioresour. Technol. 83 (2002) 37–46.

[3]   H. Xie, D. Zhang, G. Mao, F. Wang, A. Song, Availability of lignocellulose from

forestry waste for use as a biofuel in China, 3 Biotech. 8 (2018) 234.

[4]   J. Sarkar, S. Bhattacharyya, A review on biomass-based hydrogen production and

potential applications, Int. J. Energy Res. 36 (2012) 415–455.

[5]   M.A. Perea-Moreno, E. Samerón-Manzano, A.J. Perea-Moreno, Biomass as renewable energy: Worldwide research trends, Sustainability. 11 (2019) 863.

[6]   J.N. Janevski, B. V. Stojanović, M.S. Laković, M.M. Stojiljković, D.M. Mitrović, Wood biomass in Serbia – Resources and possibilities of use, Energy Sources, Part B Econ. Plan. Policy. 11 (2016) 732–738.

[7]   S. Chauhan, Biomass resources assessment for power generation: A case study from Haryana state, India, Biomass and Bioenergy. 34 (2010) 1300–1308.

[8]   F. Präger, S. Paczkowski, G. Sailer, N.S.A. Derkyi, S. Pelz, Biomass sources for a sustainable energy supply in Ghana – A case study for Sunyani, Renew. Sustain. Energy Rev. 107 (2019) 413–424.

[9]   E. Părpăriţă, M. Brebu, M. Azhar Uddin, J. Yanik, C. Vasile, Pyrolysis behaviors of various biomasses, Polym. Degrad. Stab. 100 (2014) 1–9.

[10]   J. Dai, H. Cui, J.R. Grace, Biomass feeding for thermochemical reactors, Prog. Energy Combust. Sci. 38 (2012) 716–736.

[11]   D. Ilic, K. Williams, R. Farnish, E. Webb, G. Liu, On the challenges facing the handling of solid biomass feedstocks, Biofuels, Bioprod. Biorefining. 12 (2018) 187–202.

[12]   A. Ramírez-Gómez, Research needs on biomass characterization to prevent handling problems and hazards in industry, Part. Sci. Technol. 34 (2016) 432–441.

[13]   D. Barletta, R.J. Berry, S.H. Larsson, T.A. Lestander, M. Poletto, Á. Ramírez-Gómez, Assessment on bulk solids best practice techniques for flow characterization and storage/handling equipment design for biomass materials of different classes, Fuel Process. Technol. 138 (2015) 540–554.

[14]   L. Massaro Sousa, M.C. Ferreira, Analysis of the Performance of an L-Valve Feeding Spent Coffee Ground Powders into a Circulating Fluidized Bed, Powder Technol. 362

(2020) 759–769.

[15]   L. Massaro Sousa, M.C. Ferreira, On the Performance of a Spouted Bed type Device for Feeding Spent Coffee Grounds to a Circulating Fluidized Bed Reactor, Chem. Eng. Res. Des. 160 (2020) 31–38.

[16]   M.O. Guedon, T. Baron, C.L. Briens, T.M. Knowlton, Intermittent injection of prepolymer in a pressurized fluidized bed, Powder Technol. 78 (1994) 25–32.

[17]   F.M. Berruti, C.L. Briens, Novel intermittent solid slug feeder for fast pyrolysis reactors: Fundamentals and modeling, Powder Technol. 247 (2013) 95–105.

[18]   F.M. Berruti, L. Ferrante, F. Berruti, C. Briens, Optimization of an intermittent slug injection system for sawdust biomass pyrolysis, Int. J. Chem. React. Eng. 7 (2009) 1–10.

[19]   F.M. Berruti, L. Ferrante, C.L. Briens, F. Berruti, Pyrolysis of cohesive meat and bone meal in a bubbling fluidized bed with an intermittent solid slug feeder, J. Anal. Appl. Pyrolysis. 94 (2012) 153–162.

[20]   C.S. Lira, F.M. Berruti, P. Palmisano, F. Berruti, C. Briens, A.A.B. Pécora, Fast pyrolysis of Amazon tucumã (Astrocaryum aculeatum) seeds in a bubbling fluidized bed reactor, J. Anal. Appl. Pyrolysis. 99 (2013) 23–31.

[21]   F. Wang, Z. Yu, Q. Marashdeh, L.S. Fan, Horizontal gas and gas/solid jet penetration in a gas-solid fluidized bed, Chem. Eng. Sci. 65 (2010) 3394–3408.

[22]   L. Massaro Sousa, M.C. Ferreira, Spent coffee grounds as a renewable source of energy: An analysis of bulk powder flowability, Particuology. 43 (2019) 92–100.

[23]   L. Massaro Sousa, M.C. Ferreira, Densification behavior of dry spent coffee ground powders: Experimental analysis and predictive methods, Powder Technol. 357 (2019) 149–157.

[24]   J. Dhiman, A. Shrestha, O. Fasina, S. Adhikari, B. Via, T. Gallagher, Physical,

ignition, and volatilization properties of biomass feedstocks dusts, Trans. ASABE. 58 (2016) 1425–1437.

[25] K. Tannous, P.S. Lam, S. Sokhansanj, J.. R. Grace, Physical Properties for Flow Characterization of Ground Biomass from Douglas Fir Wood, Part. Sci. Technol. 31 (2013) 291–300.

[26] E. Abdullah, D. Geldart, The use of bulk density measurements as a flowability indicator, Powder Technol. 102 (1999) 151–165.

[27] L. Massaro Sousa, M.C. Ferreira, Q.F. Hou, A.B. Yu, Feeding Spent Coffee Ground Powders with a Non-Mechanical L-valve: Experimental Analysis and TFM Simulation, Powder Technol. 360 (2020) 1055–1066.

[28] W.C. Yang, T.M. Knowlton, L-valve equations, Powder Technol. 77 (1993) 49–54.

[29] J.R. Grace, A.A. Avidan, T.M. Knowlton, Circulating Fluidized Beds, 1st ed., Chapman & Hall, 1997.

Table A1. Experimental data for the injection assays.

Exp.	Powder	P (kPa)	M (kg)	U (m/s)	U_G (m/s)	R (%)	Δt (s)	V_A (-)	X (%)	U_T (m/s)	G_S (kg/m²s)	ε_s (-)
1	S_2	300	0.003	0	0	3.1	0.096	2.81	0	16.1	100 ± 10	0.07
2	S_2	300	0.006	0	0	2.7	0.134	2.76	0	11.3	138 ± 2	0.10
3	S_2	300	0.012	0	0	5.7	0.161	2.66	0	9.1	230 ± 10	0.14
4	S_2	300	0.012	4.4	0	5.6	0.167	2.66	9.2	9.6	216 ± 6	0.14
5	S_2	400	0.012	4.4	0	2.6	0.147	3.55	6.2	14.2	250 ± 20	0.12
6	S_2	500	0.012	4.4	0	0.9	0.134	4.44	4.6	19.2	284 ± 8	0.11
7	S_2	300	0.012	17.5	0	5.7	0.127	2.66	23.4	15.1	285 ± 9	0.13
8	S_2	300	0.012	26.2	0	7.0	0.128	2.66	31.7	16.8	280 ± 30	0.12
9	S_1, S_3	300	0.003	0	0	5.7, 0.7	0.115, 0.105	2.81, 2.80	0, 0	13.5, 14.7	80 ± 10, 90 ± 20	0.08, 0.08
10	S_1, S_3	300	0.012	4.4	0	6.3, 38.8	0.169, 0.277	2.65, 2.64	9.3, 14.5	9.5, 6.1	210 ± 20, 90 ± 20	0.14, 0.11
11	S_1, S_3	300	0.012	17.5	0	6.7, 21.6	0.113, 0.199	2.65, 2.64	21.5, 32.6	16.5, 10.8	320 ± 10, 150 ± 40	0.13, 0.11
12	S_1, S_3	400	0.012	4.4	0	0.9, 8.3	0.133, 0.189	3.54, 3.51	5.7, 7.9	15.5, 11.1	290 ± 20, 186 ± 4	0.13, 0.12
13	S_2	300	0.012	17.5	0.29	5.7	0.108	2.66	20.7	17.1	330 ± 30	0.13
14	S_2	300	0.012	17.5	0.48	6.0	0.114	2.66	21.5	16.4	320 ± 30	0.13
15	S_2	300	0.012	17.5	0.77	5.3	0.133	2.66	24.3	14.6	270 ± 30	0.13
16	S_2	300	0.012	17.5	0	2.6	0.120	2.66	22.4	15.8	320 ± 40	0.13
17	S_2	300	0.012	17.5	0.14	3.5	0.100	2.66	19.4	18.2	370 ± 50	0.13
18	S_2	300	0.012	17.5	0.29	3.3	0.134	2.66	24.4	14.5	280 ± 50	0.13
19	S_2	300	0.012	17.5	0.48	3.2	0.107	2.66	20.5	17.3	350 ± 20	0.13
20	S_2	180	0.003	0	0	9.3	0.112	1.68	0	8.3	80 ± 10	0.09
21	S_2	200	0.003	0	0	2.7	0.115	1.87	0	9.0	80 ± 10	0.09
22	S_2	250	0.003	0	0	2.0	0.100	2.34	0	12.9	90 ± 10	0.08
23	S_2	400	0.003	0	0	0.7	0.049	3.74	0	42.0	190 ± 20	0.06
24	S_2	500	0.003	0	0	0.3	0.045	4.68	0	57.2	210 ± 20	0.06
25	S_2	300	0.018	0	0	8.8	0.173	2.57	0	8.2	300 ± 20	0.17
26	S_2	500	0.018	4.4	0	0.2	0.173	4.28	6.1	14.5	330 ± 20	0.14
27	S_2	500	0.024	4.4	0	2.9	0.212	4.12	7.6	11.6	350 ± 20	0.16
28	S_2	500	0.026	4.4	0	1.1	0.219	4.06	8.0	11.1	370 ± 30	0.17
29	S_2	200	0.006	0	0	9.3	0.150	1.84	0	6.7	115 ± 10	0.12